Eur Biophys J (2008) 38:99–110
DOI 10.1007/s00249-008-0363-3

ORIGINAL PAPER

# Effects of oxidation, pH and lipids on amyloidogenic peptide structure: implications for fibril formation?

**Andrew Hung · Michael D. W. Griffin · Geoffrey J. Howlett · Irene Yarovsky**

Received: 24 April 2008 / Revised: 1 August 2008 / Accepted: 4 August 2008 / Published online: 4 September 2008


**Abstract** We have performed experimental and computational studies to investigate the influences of phospholipids, methionine oxidation and acidic pH on amyloid fibril formation by a peptide derived from human apolipoprotein C-II (apoC-II), a known component of proteinaceous atherosclerotic plaques. Fibril growth monitored by thioflavin T fluorescence revealed inhibition under lipid-rich and oxidising conditions. We subsequently performed fully-solvated atomistic molecular dynamics (MD) simulations of the peptide monomer to study its conformations under both fibril favouring (neutral and low pH) and inhibiting (lipid-rich and oxidising) conditions. Examination of the chain topology, backbone hydrogen-bonding patterns and aromatic sidechain orientations of the peptide under different conditions reveals that, while the peptide adopts similar structures under the fibril-favouring conditions, significantly different structures are obtained under fibril-disruptive conditions. Based on our results, we advance hypotheses for the roles of peptide conformation on aggregation and fibrillisation propensities.

## Introduction

A number of debilitating human disorders, including Alzheimer's, Parkinson's, and the prion diseases, are characterised by the extracellular deposition of insoluble aggregates composed of proteins and other biomolecules (Dobson 2002). Although the composition of these insoluble biomolecular aggregates vary depending on their physiological location, a significant portion is comprised of proteins in a functionally inactive fibrillar form, known as amyloid fibrils. These fibrils are generally considered as self-assembled and misfolded proteins formed by intermolecular backbone-backbone hydrogen bonding in a cross-$\beta$ pattern, with the H-bonds perpendicular to the long axis of the fibrils (Nelson and Eisenberg 2006). Protein aggregation and deposition also occurs in atherosclerotic plaques (Mak et al. 2002) where the co-localisation of specific proteins with serum amyloid P suggests the presence of amyloid fibrils (Stewart et al. 2007). One significant component of atherosclerotic plaques is apolipoprotein C-II (apoC-II), a 79-residue protein involved in lipid metabolism. ApoC-II adopts a primarily α-helical structure in the presence of lipid mimetics (MacRaild et al. 2001, 2004; Zdunek et al. 2003). However, under lipid-depleted conditions, apoC-II readily forms homogeneous fibrils with a "twisted ribbon" morphology and all of the characteristics of amyloid fibrils (Hatters et al. 2000). Hydrogen/deuterium exchange and proteolysis studies identified core regions within these fibrils postulated to drive fibril formation (Wilson et al. 2007). Consistent with this hypothesis was the observation that a tryptic peptide derived from a core region, apoC-II$_{56–76}$, and a related shorter peptide, apoC-II$_{60–70}$, retained the ability of the full-length protein to form fibrils. Several solution conditions, including the presence of auxillary proteins (Hatters and Howlett 2002; Hatters et al. 2001; Powers et al. 2007), macromolecular crowding agents (Hatters et al. 2002) and the presence of phospholipids below and above the critical micelle concentration (CMC) alter the kinetics of apoC-II fibril formation and fibril morphology

A. Hung · I. Yarovsky (✉)
School of Applied Sciences, RMIT University,
GPO Box 2476V, Melbourne, VIC 3001, Australia
e-mail: irene.yarovsky@rmit.edu.au

M. D. W. Griffin · G. J. Howlett
Biochemistry and Molecular Biology,
Bio21 Molecular Science and Biotechnology Institute,
University of Melbourne, Melbourne, VIC 3010, Australia

(Griffin et al. 2008; Hatters et al. 2001). Other environmental conditions, including pH, and methionine oxidation, are known to affect fibril formation by other proteins, including A$\beta$ (Hou et al. 2002), $\alpha$-synuclein (Fink 2006), transthyretin (Maleknia et al. 2006), and prion protein (Bergstrom et al. 2007). Understanding the environmental factors which affect fibril formation in apoC-II, and in particular, those which inhibit fibril formation or result in dissolution of pre-formed, mature fibrils, is important to the development of possible therapeutic strategies against degenerative conformational diseases such as atherosclerosis.

In addition to knowing, at a phenomenological level, the conditions which affect fibril formation, knowledge of the peptide conformations under conditions which render it either more or less prone to aggregation is vital to understanding the factors which contribute to the fibrillisation process. However, atomic structures of peptide monomers are difficult to obtain using current experimental methods, although limited structural information can be deduced from techniques such as circular dichroism and NMR. Atomistic molecular dynamics simulations can complement experimental studies by enabling direct observation of the conformations and dynamics exhibited by peptides in different explicit solvent environments under controlled conditions. Numerous computational studies have been performed using all-atom models on amyloidogenic peptides and proteins, including the monomeric structures of A$\beta$1-40 and 42 (Luttmann and Fels 2006; Tomaselli et al. 2006) and its shorter derivative peptides (Baumketner et al. 2006; Baumketner and Shea 2006, 2007; Daidone et al. 2004; Milner-White et al. 2006; Tarus et al. 2006); $\beta$(2)-microglobulin (Nishino et al. 2005) and the H1 peptide (Daidone et al. 2005). In addition to water environments, a number of MD studies have investigated the effects of solvent environment on monomer structures of A$\beta$ (Kamiya et al. 2007; Wei and Shea 2006) and other peptides including B18 fusion peptide (Knecht et al. 2007) and HIV-1 gp41 (Gordon et al. 2004). The effects of single-residue mutations (Ma and Nussinov 2002), deletions (Santini and Derreumaux 2004), varying pH (Flock et al. 2006a; Han and Wu 2007; Khandogin et al. 2006), termini charge states (Flock et al. 2006a) and methionine oxidation (Triguero et al. 2008) on monomeric structures and subsequent implications for oligomer formation have also been explored.

In the current work, we combine experimental and computational techniques to study the effects of environment on the fibril formation behaviour of an 11-residue peptide derived from the core region of apoC-II (segment 60–70), known to form fibrils independently. Short peptide fibrils share the backbone structural properties of those derived from full-length proteins, and so understanding the mechanisms of peptide fibrillisation and inhibition by environmental factors serves as a foundation for understanding the aggregation of larger proteins. We use thioflavin T (ThT) fluorescence to monitor the time course of fibril formation of the peptide under a number of conditions known to influence the fibril formation behaviour of the full-length protein. We subsequently employ atomistic MD simulations to examine the conformations and dynamics of the apoC-$II_{60–70}$ peptide under fibrillisation-prone (neutral and low pH) and inhibited (oxidised M60) states, as well as in the presence of free, solvated 1,2 dipentanoyl-*sn*-glycero-3-phosphocholine (D5PC) lipids. These results enable comparison between the properties of the peptide under a range of conditions both favourable and inhibitory to fibrillisation, and elucidate some of the features of the peptide structure which render it more (or less) likely to form fibrils, with the results thereby serving as a possible predictive measure of fibrillogenicity.

## Methods

### Peptide synthesis and ox-M60 peptide preparation

ApoC-$II_{60–70}$ (MSTYTGIFTDQ) was assembled fully manually by Bio21 Peptide Technologies (Vic, Australia) using Fmoc-solid phase synthesis. The purity (>95%) and identity of the peptide were confirmed by reversed-phase high performance liquid chromatography (HPLC) and mass spectrometry using a Q-TOF LC mass spectrometer (Agilent Technologies, USA). Ox-M60 peptide was prepared by incubation of synthetic apoC-$II_{60–70}$ with 0.1% $H_2O_2$ in 5 M guanidine hydrochloride, 10 mM Tris.HCl, pH 8.0 for 2 hours. The product was purified by HPLC and lyophilised. The addition of 16 mass units to the molecular mass of the synthetic peptide, corresponding to the formation of methionine sulphoxide at position 60, was confirmed by mass spectrometry using a Q-TOF LC mass spectrometer (Agilent Technologies, USA), and the purity was estimated at >95%. Concentrated stocks of apoC-$II_{60–70}$ and ox-M60 ($\sim$24 mM) were maintained in 5 M guanidine hydrochloride, 10 mM Tris–HCl, pH 8.0 to prevent aggregation of the peptides. The concentration of each stock solution was confirmed by UV absorbance at 280 nm (Molar extinction at 280 nm in 5 M guanidine hydrochloride = 1,280 $M^{-1}$ $cm^{-1}$).

### Experimental fibril preparation and ThT assays

In all cases fibril formation was initiated by dilution of concentrated peptide stocks to 240 µM peptide in buffer, thereby reducing the guanidine hydrochloride concentration to levels where it exerts little effect on the peptide. Fibril formation was conducted at room temperature (22°C). For experiments examining the effect of lipid, apoC-$II_{60–70}$ was diluted with 100 mM sodium phosphate

buffer, pH 7.4 in the presence or absence of the stated concentrations of D5PC. For experiments examining the effect of pH, apoC-$II_{60–70}$ was diluted with 100 mM sodium phosphate, 50 mM citrate buffer, at the stated pH values. For experiments examining the effect of methionine oxidation, ox-M60 peptide was diluted with 100 mM sodium phosphate buffer, pH 7.4. The ThT fluorescence assays were performed as follows. At fixed time points after initialisation of fibril formation, 20 µl aliquots of the fibril suspension were removed and mixed thoroughly with solutions of ThT in a 96-well micro-titre plate (final concentration 10 µM ThT in 100 mM sodium phosphate buffer, pH 7.4, 250 µl final volume). Fluorescence intensities were measured using an $f_{max}$ fluorescence plate reader with excitation and emission filters of 444 and 485 nm, respectively. All measurements were made in duplicate.

### Molecular dynamics simulation parameters and set-ups

Molecular dynamics simulations were performed under constant particle number, pressure and temperature (NPT) conditions using GROMACS version 3.3 (Lindahl et al. 2001; Van der Spoel et al. 2005) and the GROMOS96 forcefield (Gunsteren et al. 1996) with the 43a1 parameter set. Forcefield parameters for the oxidised methionine sidechain were derived from those of DMSO for the GROMOS96FF. Forcefield parameters for the D5PC lipid molecules were derived from those of Berger et al. (1997). The simulation trajectory was integrated using time steps of 2 fs. Particle mesh Ewald (PME) summation (Darden et al. 1993) was employed for evaluation of long-range electrostatics, while a cut-off radius of 1.4 nm was specified for short-range non-bonded interactions. Covalent bond lengths were constrained via the LINCS algorithm (Hess et al. 1997). The simulation systems were maintained at 300 K and 1 Bar using Berendsen temperature and pressure coupling (Berendsen et al. 1984). Analyses of MD trajectories were performed using the GROMACS suite of analysis tools. Visualisation of molecular graphics were performed using VMD (Humphrey et al. 1996). Protein secondary structure was obtained using the DSSP methodology (Kabsch and Sander 1983).

The native neutral pH, low pH and the oxidised methionine peptides (hereafter abbreviated to ox-M60) systems were constructed by placing the peptides in a fully-solvated 40 $Å^3$ simulation cell with charge-neutralising counterions. The "low-pH" peptide was simulated by protonating the D69 sidechain and the C-terminal carboxylate groups. This approximates the protonation states of these functional groups of the peptide under the low pH conditions studied experimentally since the aspartate side chain is expected to be protonated at pH 4.0 and both the aspartate and C-terminal carboxyl groups will be protonated at pH 2.5 (Thurlkill et al. 2006). Simulations with lipids were initially set up with four D5PC lipids placed at approximately 10 Å separations from the peptide. This particular number of lipids was chosen because in our ThT fluorescence experiments, it was revealed that peptide:lipid ratios of 1:4 was sufficient to result in fibril inhibition (see "Results"); thus, it appears to be the minimum lipid concentration required for significant retardation of fibrillisation, and it was, therefore, desirable to use simulations to examine the structure changes which this concentration of lipids causes the peptide to result in its loss of fibrillogenicity. All systems were simulated using standard protocol: the initial peptide structures were extracted from the NMR-acquired PDB structure 1SOH (MacRaild et al. 2004), energy-minimised using the steepest-descent algorithm implemented in Gromacs 3.3 in vacuo, with another round of energy minimisation performed after addition of solvation water molecules, counterions and lipids (for the D5PC simulation). Subsequent "solvent equilibration" MD simulations of 100 ps each were performed for all of the systems, in which the heavy atoms of the peptides were positionally restrained using restraint constants of 1,000 $kJ^{-1}$ $mol^{-1}$ $nm^{-2}$, while the waters and counterions were free to undergo unrestrained dynamics. Fully unrestrained simulations were subsequently performed for all of the systems, with simulation times up to ~620 ns per system. A combined simulation time of approximately 2,300 ns was obtained.

## Results

### ThT fluorescence time course

Fibril formation by apoC-$II_{60–70}$ was monitored by the induction of ThT fluorescence (Fig. 1a–c). Figure 1a illustrates the effects of D5PC lipids on the fibrillisation of the peptide. The ThT fluorescence profile for the un-oxidised apoC-$II_{60–70}$ alone has a sigmoidal shape characteristic of a relatively short, initial lag phase followed by rapid fibril growth (filled circles; for electron micrographs of fibrils see Wilson et al. 2007). Increasing peptide:lipid molar ratios ranging from 1:1 (240 µM) to 1:6 (1.44 mM), caused progressive inhibition of fibril formation with complete inhibition at the sub-micellar concentration of 1.44 mM, over the time course studied, with a ratio of 1:4 sufficient to cause fibril inhibition up to ~24 h, with a more gradual fibrillisation commencing after ~30 h incubation. Oxidation of M60 resulted in complete fibril inhibition, as illustrated in Fig. 1b, with the ox-M60 peptide exhibiting negligible ThT fluorescence over the entire duration of the experiment. Furthermore, we have monitored fibril formation at acidic pH of 2.5 and 4.0 (Fig. 1c). Comparison of the ThT fluorescence curves acquired at the pH values studied suggest that

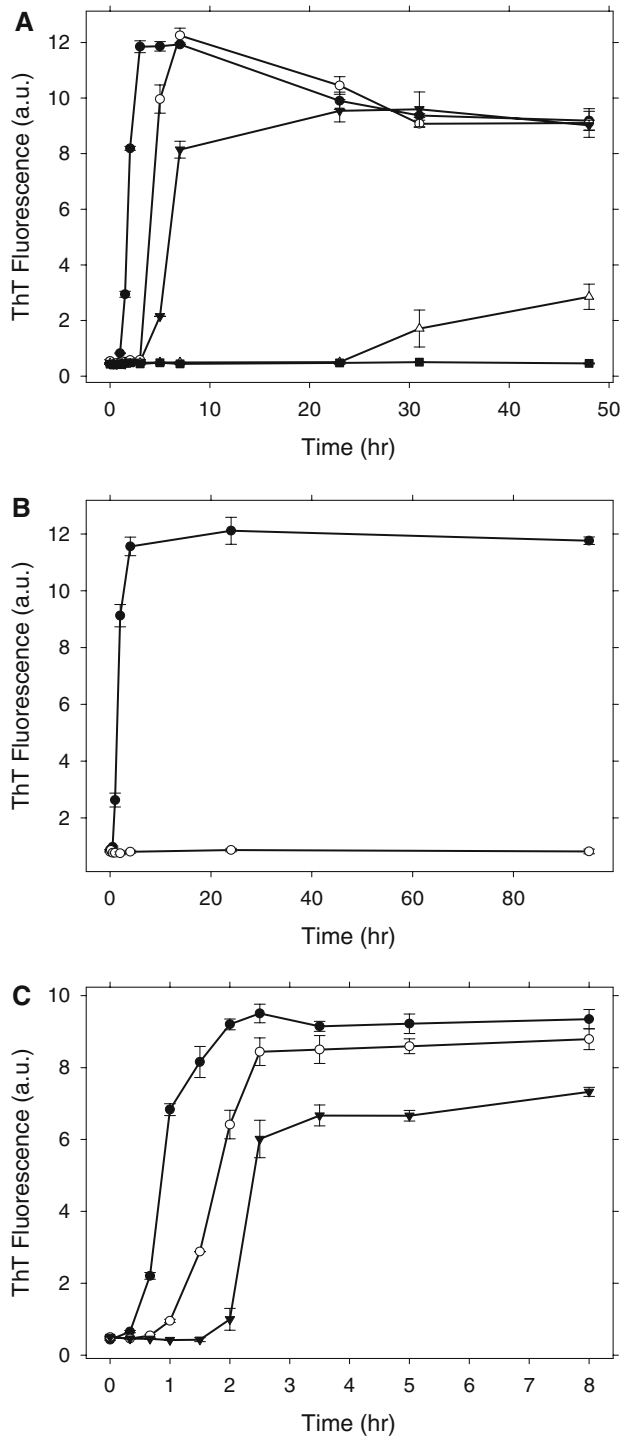


**Fig. 1** The effects of lipid, methionine oxidation, and pH on fibril formation by apoC-II (60–70). **a** ApoC-II (60–70) fibril formation was initiated in the absence (*filled circles*) and presence of D5PC at concentrations of 240 μM (*open circles*), 480 μM (*inverted filled triangles*), 960 μM (*open triangles*), and 1440 μM (*filled squares*). **b** Fibril formation was initiated by native apoC-II (60–70) (*filled circles*) and ox-M60 peptide (*open circles*). **c** ApoC-II (60–70) fibril formation was initiated at pH 7.4 (*filled circles*), pH 4.0 (*open circles*) and pH 2.5 (*filled triangles*). Fibril formation was initiated at 240 μM peptide concentration and the time course of fibril formation was monitored by ThT fluorescence. *Error bars* indicate standard error

fibril formation is not prevented under acidic conditions; however, the lag phase prior to fibrillisation is pH-dependent, with the longest lag phase observed at pH 2.5, followed by increasingly shorter ones at 4.0 and 7.4. Thus, the more acidic the solution, the slower the kinetics of fibril growth.

## Overall peptide structural characteristics

We describe results from our MD simulations in the following sections. The overall peptide structure may be described in terms of simple geometric parameters, namely the peptide extension (measured as distance between the N- and C-termini) and sphericity (radius of gyration, $R_g$). Plots of chain extension with respect to $R_g$ are shown in Fig 2a–c, with the data points acquired by uniform sampling of frames (snapshots) from the simulated trajectories. These plots indicate the "tertiary structure"—the overall fold—of the peptides exhibited during the simulations, as well as the approximate extent of sampling of the conformational landscape. Inspection of Fig. 2a indicates that the fibril-favoured neutral and low pH systems are qualitatively similar, with frequent sampling (evidenced by tight clusters of data points) around two main conformational basins at distance = 0.5 nm and $R_g$ = 0.55 nm (hereafter, simplified to e.g. (0.5, 0.55)) and at (0.9, 0.55). Ribbon representations of typical structures at these basins are illustrated in the figures. Both structure types resemble hairpins, with the turn region located in the proximity of G65. This is perhaps not surprising, given that glycine residues are well-known to impart chain flexibility in proteins and peptides by nature of its lack of a sidechain. We note that a similar turn region was identified in MD simulations of the peptide derived from residues 56 to 76 (Legge et al. 2007), suggesting that this may be a common structural feature in not only the 11-residue peptide, but also larger peptides which incorporate this segment, as well as in the intact protein. The structure corresponding to the former cluster indicates a "tight" structure, with the termini close to each other and inter-strand H-bonding present (see "Discussion" below), while the latter indicates a "looser" structure, with the termini further parted, but with the hairpin structure intact. The low pH peptide data points exhibit a greater spread, indicative of enhanced chain flexibility relative to the neutral pH system. It also samples the very low inter-termini distances (i.e. below ~0.4 nm) much more rarely than the neutral pH peptide, this being likely to be due to the lack of strong electrostatic attraction between the termini (the C-terminus is neutralised).

The oxidised methionine (ox-M60) peptide exhibits different behaviour compared to those of the native peptides discussed above (Fig. 2b), with two general conformational basins at (0.5, 0.6) and at (1.2, 0.5). The former adopts a

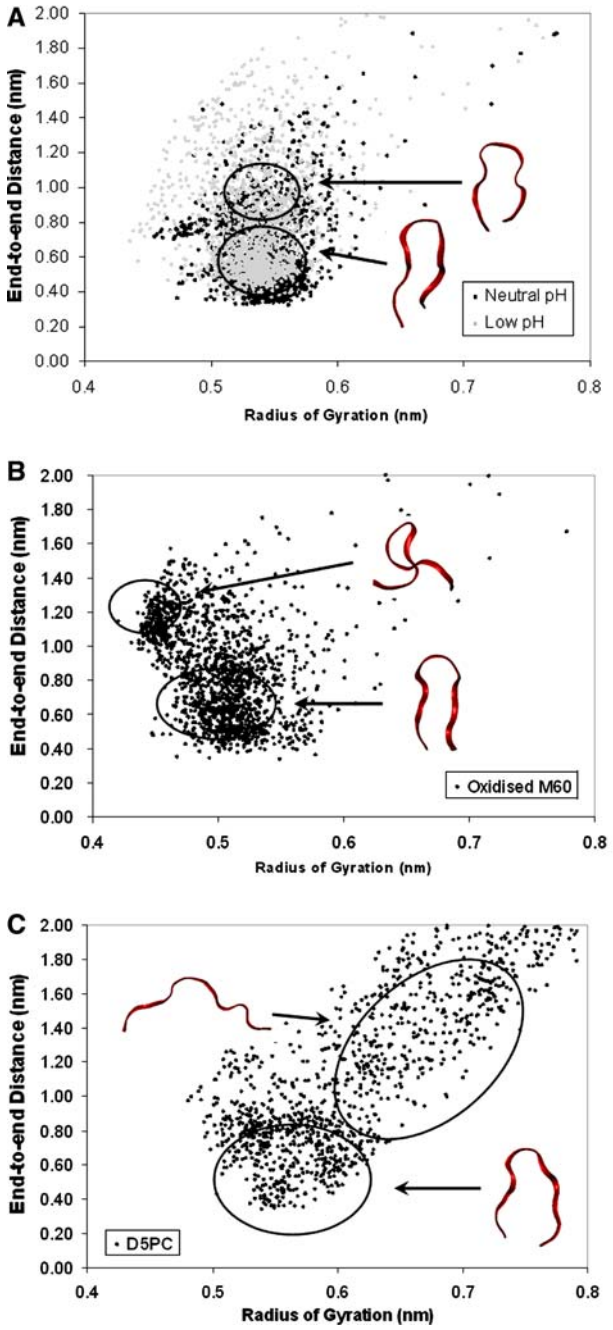


**Fig. 2** Peptide inter-termini (end-to-end) distance with respect to radius of gyration ($R_g$) for the four systems, with data points obtained at uniform separation from each trajectory, for the (**a**) neutral and low pH system; (**b**) oxidised M60, and (**c**) system with free D5PC surrounding the peptide. Ribbon graphics of the peptides corresponding to indicated regions of conformational space sampled are *inset*, and were selected from the trajectories at frames in which the peptides adopted the structures characteristic of the region circled on the distance-$R_g$ plots

*twisted* hairpin structure, qualitatively similar to the (0.9, 0.55) cluster identified for the native peptides, while the latter, unique to ox-M60, has an $R_g$ characteristic of a hairpin-like structure, but also has much higher end-to-end distances. This latter conformation is largely manifested in the final ~200 ns of the trajectory, in which the peptide adopts a "tied-ribbon"-like configuration, in which M60 forms apparently strong interactions with S61 and T62 (see below), making the peptide more spherical in appearance and yet maintaining the termini distances at a relatively wide separation; this is quite different from the tighter hairpin structures common to the non-oxidised peptides. Finally, for the lipid system (Fig. 2c), we observe a much broader distribution of conformations, with a loose cluster centred at (0.55, 0.6), and many instances of extended chain structures which are not sampled at all in the lipid-free systems. This extension is due to persistent interactions with lipids, which serve to pry open the peptide chain (discussed below).

## Secondary structures and sidechain interactions

Inspection of the secondary structure with respect to time shows that the fibril-favoured, native peptides at neutral and low pH (Fig. 3a, b, respectively) are qualitatively similar, with intramolecular backbone H-bonding between the strands of the $\beta$-hairpin (residues 62–63 with that of 67–68) present approximately 30% of the total trajectory, and a random coil (though hairpin-like) structure adopted for the remainder of the simulation. The principal difference between the neutral and low pH peptides lie in the nature of their fluctuations. While the backbone H-bonds of the neutral pH peptide undergo rapid fluctuations between H-bonded and non-H-bonded states (as evidenced by frequent interruptions in the "red" regions on the DSSP map, Fig. 3a), the low pH peptide undergoes lower frequency, discrete fluctuations between $\beta$-stranded (30–150 ns, 325–375 ns, 425–525 ns) and random coil states, with relatively minor "intra-state" fluctuations, thus producing more tightly spaced "red" regions (Fig. 3b). Thus overall, the $\beta$-hairpin structure, although present in both low and neutral pH systems, appears to be more strongly maintained for the former. The origin of this difference may be partly elucidated by examination of the sidechain interactions between D69 and Y63. In the neutral pH peptide, the (negatively charged) D69 forms frequent H-bonding to the hydroxyl group of Y63 causing the aromatic ring of Y63 to slip between the two strands of the hairpin structure (illustrated by the snapshot in Fig. 4a), disrupting the backbone-backbone interstrand H-bonding, resulting in the rapid "intra-state" fluctuations observed in the DSSP plot. However, this interaction is likely to be significantly weakened in the case of the low pH system, in which the charge on D69 is neutralised by protonation. Thus, unlike the neutral pH peptide, Y63 does not slip in between the (backbone H-bonded) strands, allowing H-bonding to be more persistently maintained.

Far less $\beta$-hairpin structures are observed for the fibril-inhibited peptides (Fig. 3c, d); the peptides are in extended,

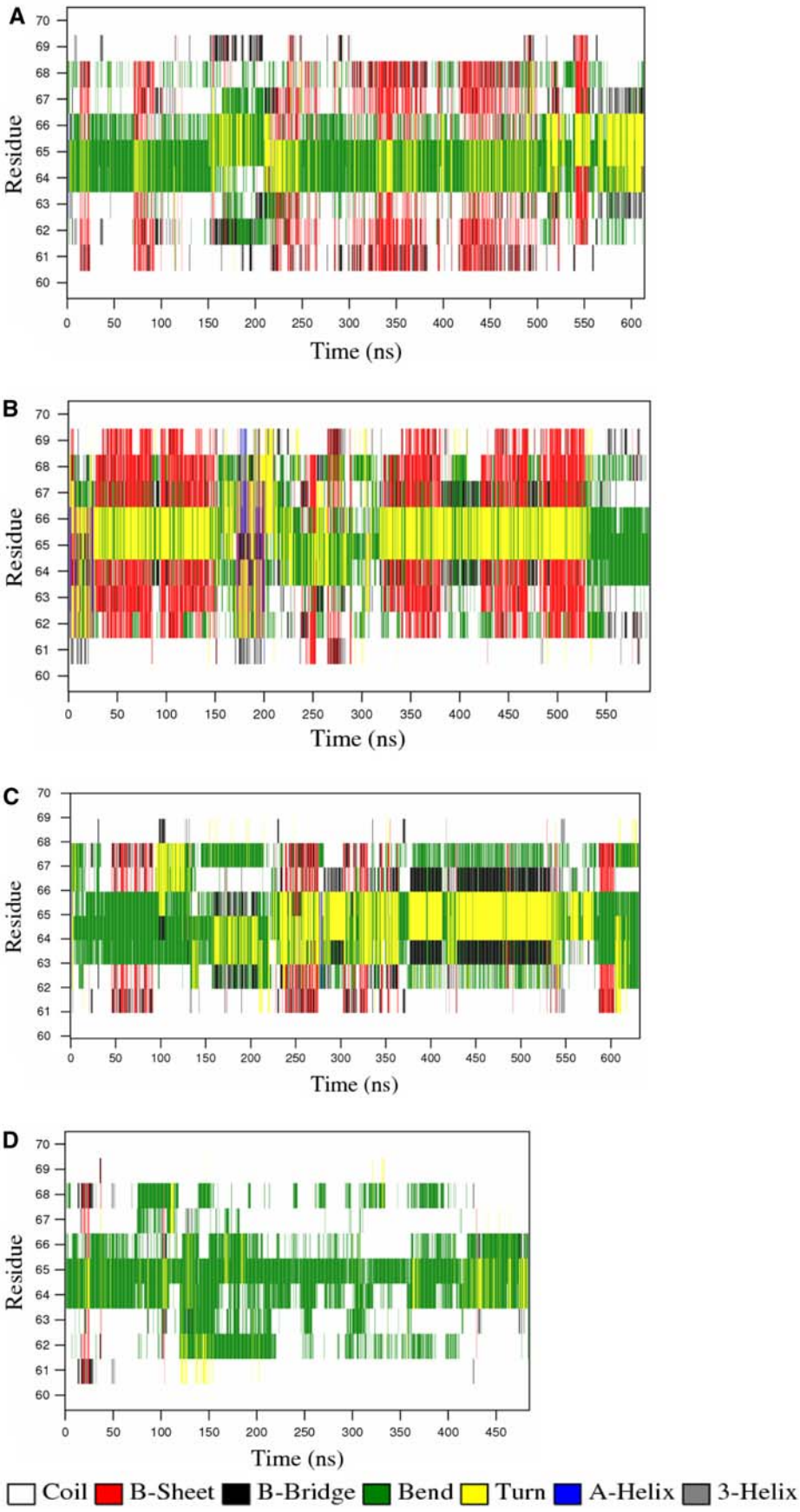


**Fig. 3** Secondary structures for each residue with respect to simulation time for the (**a**) neutral pH, (**b**) low pH, (**c**) oxidised M60 and (**d**) D5PC systems. Assignments for each residue *colour-coded* as indicated

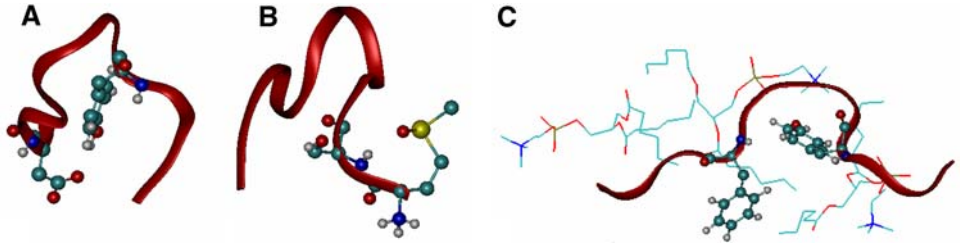


**Fig. 4** Peptide structures taken from trajectory snapshots for illustration of key sidechain interactions discussed in text. **a** Neutral pH peptide with Y63-D69 H-bonding interaction which disrupts hairpin integrity; **b** oxidised M60 sidechain with persistent H-bonding to S61 backbone; **c** stabilisation of the peptide in extended conformations by lipid tail hydrophobic contacts with Y63 and F67 rings. Sidechains of particular importance for their influence on overall peptide structure are displayed in CPK representation

random coil conformations for much of the simulation time. While lipid interactions serve to stabilise the peptide in extended conformations for the D5PC system, more surprising perhaps is that for the ox-M60 peptide, a single additional oxygen atom alone is apparently capable of altering its conformational sampling relative to the original peptide. This can be partly understood by examining the H-bonding interactions formed between the sidechain of the oxidised M60 and the remainder of the peptide during the course of the simulation. We calculate the H-bond existence map for this interaction, shown in Fig. 5, in which individual H-bonds (differentiated by the identities of the 3 atoms involved) are labelled by index according to order of first appearance in the trajectory, with a red line indicating the presence of the respective H-bond. In this calculation, a H-bond is defined as present if potential acceptor-donor atom pairs are within 0.35 nm and the atoms comprising the triplet adopt an angle >30°. Inspection of Fig. 5 reveals that indices 12 and 11, which correspond to H-bonding between

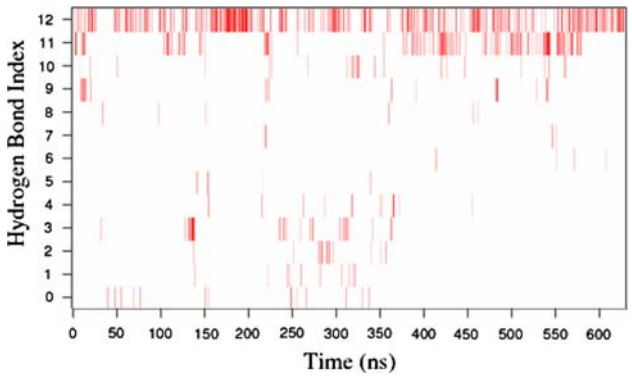


**Fig. 5** H-bond existence map for the M60 sidechain of the oxidised peptide with the rest of the protein, with respect to time. *Red lines* indicate H-bond existence for particular interactions labelled by index, in order of initial appearance in trajectory. Persistent H-bonding exists throughout the trajectory for H-bond index 12, corresponding to H-bonding between sidechain of ox-M60 and backbone NH of S61. Less persistent H-bonding occurs between ox-M60 and T62, shown as index 11. H-bonding interactions with other regions of the peptide are far less pronounced (indices 0–10)

S=O of ox-M60 and the backbone N–H of S61 (illustrated in Fig. 4b) and T62, respectively, show persistent presence of H-bonding. The former bond is apparently more persistent, being maintained (with some fluctuations) throughout the entire ~600 ns trajectory, while H-bond interactions between the M60 sidechain and other residues (i.e. besides S61 and T62) are relatively sparse. It is possible that this interaction weakens those between the two strands, especially near the termini region, through competitive H-bonding, thus making it more likely for the hairpin to "open up" and thereby adopt a relatively extended structure. This interaction is also responsible for the "twisted" appearance of the hairpin towards the N-terminus end which results in the structure shown in the inset in Figs. 2b and 4b. For the D5PC-bound peptide, the adoption of extended structures is likely due to two main factors; firstly, the optimisation of favourable hydrophobic contacts between the lipid carbon tails and the peptide aromatic rings (Fig. 4c). Additionally, the charged headgroups of the lipids form strong electrostatic interactions with the termini. The choline ($-NH_3^+$) group maintains contact with the C-terminus, while the phosphate ($-PO_4^-$) group interacts with the N-terminus. These "competitive" electrostatic interactions from the lipids may further contribute to weakening of the inter-termini contact (strongly present in the case of the neutral pH peptide), in addition to the hydrophobic contacts due to carbon tails mentioned above which, combined, lead to extension of the peptide chain throughout much of the trajectory (refer to Fig. 2c).

## Relative orientations of aromatic sidechains

The interactions between aromatic residues are known to play a critical role in aggregation (Colombo et al. 2005; Reches and Gazit 2005). For example, in the case of the IAPP motif it has been shown that the substitution of the Phe with a less hydrophobic Trp still results in self-organisation of the peptides into amyloid-like structures, whereas the Phe to Ala mutation significantly reduces their amyloidogenic potential (Wu et al. 2005). Recently,

high-resolution structures of amyloid assemblies involving aromatic interactions have been published, indicating their role in stabilising mature fibrils (Inouye et al. 2006; Makin et al. 2005). It is, therefore, reasonable to assume that the presence of two aromatic residues in apoC-II (60–70) plays an important role in the aggregation and fibrillation of this peptide. As such, we examine their configuration in the monomer with respect to fibril favouring or inhibiting conditions.

A simple measure of the potential contribution of aromatic sidechains to peptide self-assembly in solution is their solvent-accessible-surface area (SASA), which effectively determines the degree of exposure of the sidechains, and therefore, their potential capability to form intermolecular contacts. However, calculation of the SASA for the neutral pH and the ox-M60 peptide gave no statistically significant difference, with trajectory-averaged values of $2.9 \pm 0.3$ and $3.0 \pm 0.4\ \mathrm{nm}^2$, respectively. Thus, there appears to be no apparent differences in the overall degree of aromatic ring exposure for the two types of peptides, despite their experimentally-observed differences in fibril-formation, as well as their apparent differences in structure (discussed in above sections).

However, inspections of the trajectories of the neutral, low pH and ox-M60 simulations reveal that differences do exist, not in their overall exposure, but in their geometries, and in particular, the relative orientations of the Y63 and F67 sidechains with respect to the peptide backbone hairpin structure. We have quantified the relative orientations of the two sidechains by calculating the angle between the C$\alpha$–C$\gamma$ vector of Y63, and the vector composed of the same atoms from F67, with respect to simulation time for the neutral, low pH and ox-M60 peptide. Angles of less than 90° indicate that the two sidechains lie on the same "face" of the peptide hairpin structure, while angles of greater than 90° indicates the opposite; namely, that the two sidechains lie on opposite faces of the hairpin. We have also examined the angles between the C$\alpha$–C$\beta$ vectors of the two residues, which gave the same qualitative results; however, the results presented here exhibit the trend in orientation more clearly. Histograms acquired from the three time-series are displayed in Fig. 6, indicating clearly that for the native peptides, the angles adopted during the trajectory are for the most part ~150°, while for the ox-M60 peptide, the majority angle is at ~50°, with a somewhat wider, more even distribution up to ~100°. Representative structures for the two cases are illustrated in the insets of Fig. 6. In general, then, the peptides under fibril-favouring conditions tend to adopt a structure whereby Y63 and F67 lie approximately on opposite "faces" of the hairpin structure, whereas for the ox-M60 peptide, they lie on the same "face" of the hairpin. Thus, in the former case, there is more uniform distribution of aromatic ring surface area, whereas for the latter case, the distribution is asymmetric, with one face strongly hydrophobic, while the other is largely hydrophilic. Differences in aromatic ring distribution symmetry (amongst other peptide structural features) may have implications in the very different fibrillisation behaviour of the native peptide as compared with that of the oxidised methionine peptide, as discussed below.

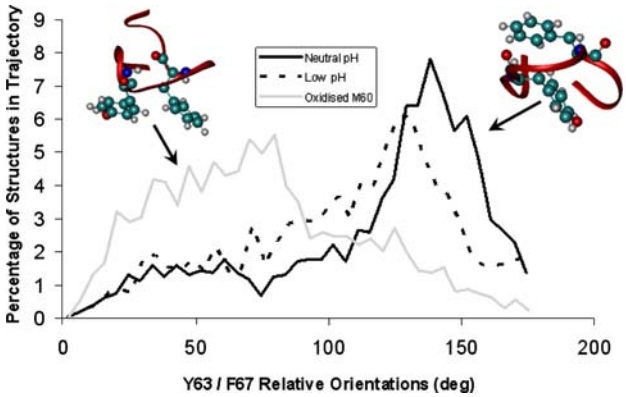


**Fig. 6** Histograms of Y63 ring orientation with respect to F67 ($x$ axis), obtained from total simulated trajectories for pure water (*filled black line*), low pH (*dashed black line*) and oxidised M60 (*grey line*); $y$ axis indicates percentage of structures for a specific orientation angle range exhibited during the trajectory. Forty bins were used over 0–180°. Each data point represents % of structures with orientation angles between $x - 4.56°$ and $x$. Angles <90° indicate existence of both rings on one side of the hairpin, while >90° indicates that rings exist on both sides. Illustrations of the relative ring orientations are *inset*

## Discussion

The peptide structures obtained from computational simulations under fibrillogenic and non-fibrillogenic conditions correlate to the fibrillsation behaviour observed experimentally (Fig. 1a–c). Namely, at both neutral and low pH, the peptide sampled similar conformations in our simulations, while our experiments revealed that at pH 7.4 and 4.0, fibril formation occurs, and at similar rates (Fig. 1b). Furthermore, while our experiments revealed that the presence of lipids at peptide:lipid ratios of 1:4 and above inhibits fibril formation (Fig. 1a), as does oxidation of M60 (Fig. 1c), our simulations reveal that the peptide structures under both these conditions differ significantly from those of the unoxidised/pure water environments. As such, our results suggest that peptide structures acquired from MD simulations of several 100 ns duration may be used as a qualitative predictor of fibrillogenicity in this peptide.

Analyses of the simulated trajectories of the four systems, each representing the apoC-II (60–70) peptide in either (experimentally-determined) fibril-favouring (neutral and low pH) and inhibitory (oxidised M60; and binding to submicellar D5PC lipids) states, revealed that although under the former conditions the peptide exhibits some

qualitatively similar backbone and sidechain conformations and dynamical fluctuations, under the latter conditions the peptide behaves quite differently, adopting different chain topologies, secondary structures and sidechain conformations. The fibrillogenic peptides tend to consistently adopt tighter, $\beta$-hairpin structures, with relatively sparse sampling of extended conformations (Fig. 2a), while the inhibited peptides exhibit a tendency to adopt a greater variety of extended strand conformations, owing to interference with intramolecular inter-terminal H-bonding from oxidised methionine sidechain (ox-M60), as well as hydrophobic and electrostatic interactions with lipids (D5PC system).

Examination of the secondary structure reveals another trend consistent with these observations. For the fibril-forming conditions, inter-strand backbone H-bonding is observed for roughly 30% of the total trajectory, during which time a $\beta$-hairpin is formed, while much lower occurrences of H-bonding is observed for the inhibited peptides, which largely adopt random coil conformations. Thus, there appears to be a trend in the secondary structure with respect to fibrillogenicity; the presence of $\beta$-hairpin structure, as observed from simulations, coincides with spontaneous peptide fibrillisation observed experimentally. Why this is so remains difficult to answer from consideration of the monomer structure alone. It is possible that the 11-residue peptide fibrils are composed of stacks of hairpins aligned along the long axis of the fibril, H-bonded via the (previously exposed, in monomeric form) backbone carbonyls and amides, as in the case of a proposed model of fibrillised transthyretin (Sinha et al. 2001), albeit in that case a larger, full-length protein. If this is the case, then it appears reasonable to assume that apoC-II$_{60–70}$ monomers under conditions which enable them to form stable $\beta$-hairpins in solution would be capable of much more rapid oligomerisation into the fibrillar form compared to conditions which disfavour $\beta$-hairpin structures; for example, the hairpin monomers may directly dock and form a fibrillar configuration; or, peptides within a disordered aggregate would simply need to undergo rigid-body rearrangements to form ordered fibrils composed of $\beta$-hairpins; whereas more significant, intramolecular structural transitions are required to form fibrils for peptides under fibril-disfavouring conditions (i.e. the monomers do not form stable hairpins in solution, but need to undergo changes to do so before forming fibrils). The relationship between $\beta$-stranded content and fibril formation is not straightforward; specifically, it does *not* appear to be the case that greater $\beta$-stranded structural persistence correlates directly with more rapid fibrillisation. The low pH simulation indicates greater $\beta$-strand persistence, evident in the distinct "blocks" of red observed in the DSSP plot (Fig. 3b), and yet exhibit slightly slower fibillisation kinetics (greater lag phase) as observed in the ThT fluorescence time traces (Fig. 1c). The delay in fibril formation at pH 4.0 and 2.5 may be due to pH effects that were not modelled in the current MD simulations. Nevertheless, our results suggest that the formation of a strand-turn-strand structure is important for aggregation, as also suggested by simulations on the 56–76 segment of apoC-II (Legge et al. 2007). In the case of the lipid-bound peptide, however, it is more likely that the lipids themselves are capable of directly altering the energetics of aggregation by forming a "lipid coat" around monomers, which then directly mediates the initial interaction between the monomers. We have explored this possible mechanism using free energy calculations (manuscript submitted).

It is of interest to note that in addition to apoC-II, it is known that oxidation of methionine appears to disrupt fibril formation for a number of amyloidogenic proteins, including prion (Bergstrom et al. 2007) and A$\beta$ (Palmblad et al. 2002). Our results suggest that oxidation influences the monomer structure through possible interference with the inter-backbone H-bonding capacity of the N-terminal region, which results in a strand structure significantly different from that of the non-oxidised peptide. Changes in monomer structure with respect to methionine chemical substitutions have also been observed in MD simulations of the A$\beta$ amyloid protein (Triguero et al. 2008). However, although a change of monomer structure may well contribute to fibril inhibition by biasing the conformational population towards non-fibril-favouring forms, we note that recent experimental evidence (Binger et al. 2008) has indicated that oxidation even of *mature fibrils* can lead to their dissociation, and subsequent re-solubilisation of the newly formed oxidised peptide. Our present results suggest that an oxidised M60 sidechain appears to be capable of disruption of peptide backbone H-bonding in its vicinity. In the case of mature fibrils, this localised disruption may be sufficient to result in significantly weakened $\beta$-stranded structure overall, leading to dissociation of the fibril.

Hydrophobic interactions between aromatic residues are known to be important in the aggregation of amyloid-forming peptides (evidenced by the aggregation of small aromatic peptides, see e.g. Gazit (2007)) as well as stabilisation of mature fibrils (Naito et al. 2004). Based on MD simulations, aromatic ring orientations of peptides have also been previously proposed to play important roles in the resultant shape of aggregates (Flock et al. 2006b). In the current work, we have examined the relative orientations of the only two aromatic amino acids in the (60–70) sequence, namely Y63 and F67, for the fibrillogenic and fibril-inhibited peptide systems, in order to acquire some further insight into the manner in which monomer structure may determine aggregation propensity. We observe a distinct bias towards symmetric distribution of aromatic surface for the fibrillogenic peptides, with Y63 and F67 sidechains situated on opposite sides of the hairpin structure, while an

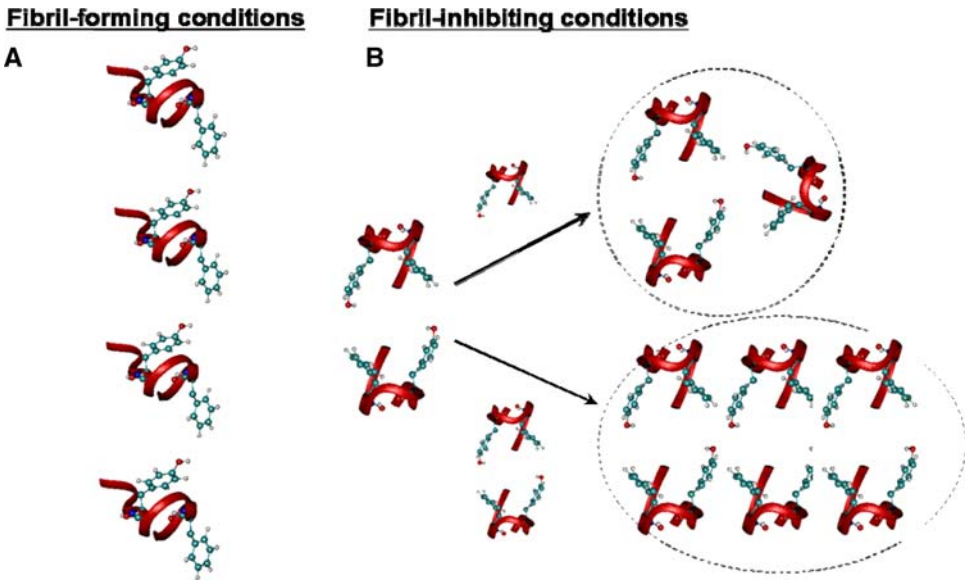


**Fig. 7** Hypothetical rigid-body model of the mechanism of initial aggregate formation for apoC-$II_{60–70}$ peptide under (**a**) favourable fibrillisation conditions and (**b**) fibril-inhibiting, oxidised M60 conditions. In the former case, many copies of the (most highly populated) monomer may form only linear aggregates, stabilised by hydrophobic contacts between their respective aromatic rings, while in the latter case, several competing aggregate formation mechanisms exist, which may result in the formation of both linear (*bottom*) and nonlinear (*top*) complexes

asymmetric distribution is observed for ox-M60, with both rings located on the same face. This particular trend may have implications for the initial stages of aggregation. We offer a possible mechanism, with two assumptions: (1) that the monomers initially self-assemble into oligomers in their solution conformation, and (2) the major driving forces behind initial aggregation are due to hydrophobic interactions. These assumptions are reasonable, given the capability of amyloidogenic peptides to self-assemble into clusters from different initial (isolated) monomer conformations; as well as the capability of di-phenylalanine to self-assemble; both of which has been demonstrated in MD simulations (Flock et al. 2006b). When the aromatic rings are facing both sides of the hairpin, we propose that this arrangement renders them capable of readily forming an energetically-favourable *linear* oligomeric complex (illustrated in Fig. 7a), stabilised by strong inter-molecular hydrophobic contacts between the aromatic sidechains, in which the constituent monomers may then undergo translational, rotational or internal structural conversion to the fibrillar form. In the case of ox-M60, there appears to be more oligomer-forming pathways involving hydrophobic ring interactions, as illustrated in Fig. 7b. While it is also possible to form an indefinitely long linear complex from this monomer structure (Fig. 7b, bottom), other complexes are also possible leading to the formation of large assemblies with hydrophobic cores, but are not necessarily one-dimensionally-extended in nature (Fig. 7b, top). The existence of multiple, competing, energetically favourable aggregation pathways, not all of which rapidly lead to linear oligomers, may be one manner in which the oxidation of M60 influences fibrillation propensity via alteration to the monomer structure. Additional experimental and theoretical investigations are required to provide further evidence for these hypotheses.

In summary, we have demonstrated experimentally that concentrations of apoC-$II_{60–70}$:D5PC of 1:4 ratios and above, as well as oxidation of M60, are capable of inducing fibril inhibition of apoC-$II_{60–70}$. We, furthermore, showed that simulations are capable of elucidating peptide structural changes due to the environmental influences studied presently, and that these changes appear to correlate with the (experimentally demonstrated) fibrillogenicity of the peptide under the same conditions, thus suggesting that MD simulations of small peptide monomers may serve to predict their environment-dependent fibril formation. Detailed examination of the MD simulation trajectories enables us to propose possible mechanisms by which peptide monomer structures may affect aggregation and subsequent fibrillisation. We are in the process of performing further studies on other factors which influence the fibrillisation of apoC-II and its derivative peptides, including mutations. Additionally, we are applying more advanced conformational sampling strategies to explore the environment-dependent oligomerisation of apoC-II peptides.

**Acknowledgments** We acknowledge the Australian Partnership for Advanced Computing (APAC) and Victorian Partnership for Advanced Computing (VPAC) for provision of computational resources, and the latter for provision of funds under the eResearch grants scheme. We also thank our colleagues at RMIT University (Sue Legge, Nevena Todorova and Akin Budi) for many helpful discussions.

## References

Baumketner A, Bernstein SL, Wyttenbach T, Lazo ND, Teplow DB, Bowers MT et al (2006) Structure of the 21–30 fragment of amyloid beta-protein. Protein Sci 15:1239–1247. doi:10.1110/ps.062076806

Baumketner A, Shea J-E (2007) The structure of the Alzheimer amyloid beta 10–35 peptide probed through replica-exchange

molecular dynamics simulations in explicit solvent. J Mol Biol 366:275–285. doi:10.1016/j.jmb.2006.11.015

Baumketner A, Shea JE (2006) Folding landscapes of the Alzheimer amyloid-beta(12–28) peptide. J Mol Biol 362:567–579. doi:10.1016/j.jmb.2006.07.032

Berendsen HJC, Postma JPM, Vangunsteren WF, Dinola A, Haak JR (1984) Molecular-dynamics with coupling to an external bath. J Chem Phys 81:3684–3690. doi:10.1063/1.448118

Berger O, Edholm O, Jahnig F (1997) Molecular dynamics simulations of a fluid bilayer of dipalmitoylphosphatidylcholine at full hydration, constant pressure, and constant temperature. Biophys J 72:2002–2013

Bergstrom AL, Chabry J, Bastholm L, Heegaard PMH (2007) Oxidation reduces the fibrillation but not the neurotoxicity of the prion peptide PrP106–126. Biochim Biophys Acta Prot Proteomics 1774:1118–1127. doi:10.1016/j.bbapap.2007.06.016

Binger KJ, Griffin MD, Howlett GJ (2008) Breaking up amyloid fibrils: methionine oxidation dissociates preformed amyloid fibrils. FEBS J 275:442

Colombo G, Daidone I, Gazit E, Amadei A, Di Nola A (2005) Molecular dynamics simulation of the aggregation of the core-recognition motif of the islet amylolid polypeptide in explicit water. Proteins 59:519–527. doi:10.1002/prot.20426

Daidone I, Amadei A, Di Nola A (2005) Thermodynamic and kinetic characterization of a beta-hairpin peptide in solution: an extended phase space sampling by molecular dynamics simulations in explicit water. Proteins 59:510–518. doi:10.1002/prot.20427

Daidone I, Simona F, Roccatano D, Broglia RA, Tiana G, Colombo G et al (2004) beta-hairpin conformation of fibrillogenic peptides: structure and alpha-beta transition mechanism revealed by molecular dynamics simulations. Proteins 57:198–204. doi:10.1002/prot.20178

Darden T, York D, Pedersen L (1993) Particle Mesh Ewald—an N.Log(N) method for Ewald sums in large systems. J Chem Phys 98:10089–10092. doi:10.1063/1.464397

Dobson CM (2002) Getting out of shape. Nature 418:729–730. doi:10.1038/418729a

Fink AL (2006) The aggregation and fibrillation of alpha-synuclein. Acc Chem Res 39:628–634. doi:10.1021/ar050073t

Flock D, Colacino S, Colombo G, Di Nola A (2006a) Misfolding of the amyloid beta-protein: a molecular dynamics study. Proteins 62:183–192. doi:10.1002/prot.20683

Flock D, Rossetti G, Daidone I, Amadei A, Di Nola A (2006b) Aggregation of small peptides studied by molecular dynamics simulations. Proteins 65:914–921. doi:10.1002/prot.21168

Gazit E (2007) Self-assembled peptide nanostructures: the design of molecular building blocks and their technological utilization. Chem Soc Rev 36:1263–1269. doi:10.1039/b605536m

Gordon LM, Mobley PW, Lee W, Eskandari S, Kaznessis YN, Sherman MA et al (2004) Conformational mapping of the N-terminal peptide of HIV-1 gp41 in lipid detergent and aqueous environments using C-13-enhanced Fourier transform infrared spectroscopy. Protein Sci 13:1012–1030. doi:10.1110/ps.03407704

Griffin MDW, Mok MLY, Wilson LM, Pham CLL, Waddington LJ, Perugini MA et al (2008) Phospholipid interaction induces molecular-level polymorphism in apolipoprotein C-II amyloid fibrils via alternative assembly pathways. J Mol Biol 375:240–256

Gunsteren WFv, Kruger P, Billeter SR, Mark AE, Eising AA, Scott WRP, Huneberger PH, Tironi IG (1996) Biomolecular simulation: the GROMOS96 manual and user guide. Biomos & Hochschulverlag AG an der ETH Zurich, Groningen/Zurich

Han W, Wu YD (2007) Molecular dynamics studies of hexamers of amyloid-beta peptide (16–35) and its mutants: influence of charge states on amyloid formation. Proteins 66:575–587. doi:10.1002/prot.21232

Hatters DM, Howlett GJ (2002) The structural basis for amyloid formation by plasma apolipoproteins: a review. Eur Biophys J Biophys Lett 31:2–8

Hatters DM, Lawrence LJ, Howlett GJ (2001) Sub-micellar phospholipid accelerates amyloid formation by apolipoprotein C-II. FEBS Lett 494:220–224. doi:10.1016/S0014-5793(01)02355-9

Hatters DM, MacPhee CE, Lawrence LJ, Sawyer WH, Howlett GJ (2000) Human apolipoprotein C-II forms twisted amyloid ribbons and closed loops. Biochemistry 39:8276–8283. doi:10.1021/bi000002w

Hatters DM, Minton AP, Howlett GJ (2002) Macromolecular crowding accelerates amyloid formation by human apolipoprotein C-II. J Biol Chem 277:7824–7830. doi:10.1074/jbc.M110429200

Hess B, Bekker H, Berendsen HJC, Fraaije JGEM (1997) LINCS: a linear constraint solver for molecular simulations. J Comput Chem 18:1463–1472. doi :10.1002/(SICI)1096-987X(199709)18:12<1463::AID-JCC4>3.0.CO;2-H

Hou LM, Kang I, Marchant RE, Zagorski MG (2002) Methionine 35 oxidation reduces fibril assembly of the amyloid A beta-(1–42) peptide of Alzheimer's disease. J Biol Chem 277:40173–40176. doi:10.1074/jbc.C200338200

Humphrey W, Dalke A, Schulten K (1996) VMD: visual molecular dynamics. J Mol Graph 14:33

Inouye H, Sharma D, Goux WJ, Kirschner DA (2006) Structure of core domain of fibril-forming PHF/Tau fragments. Biophys J 90:1774–1789

Kabsch W, Sander C (1983) Dictionary of protein secondary structure—pattern-recognition of hydrogen-bonded and geometrical features. Biopolymers 22:2577–2637. doi:10.1002/bip.360221211

Kamiya N, Mitomo D, Shea JE, Higo J (2007) Folding of the 25 residue A beta(12–36) peptide in TFE/water: temperature-dependent transition from a funneled free-energy landscape to a rugged one. J Phys Chem B 111:5351–5356. doi:10.1021/jp067075v

Khandogin J, Chen JH, Brooks CL (2006) Exploring atomistic details of pH-dependent peptide folding. PNAS USA 103:18546–18550. doi:10.1073/pnas.0605216103

Knecht V, Mohwald H, Lipowsky R (2007) Conformational diversity of the fibrillogenic fusion peptide B18 in different environments from molecular dynamics simulations. J Phys Chem B 111:4161–4170. doi:10.1021/jp0659204

Legge ES, Treutlein H, Howlett GJ, Yarovsky I (2007) Molecular dynamics simulations of a fibrillogenic peptide derived from apolipoprotein C-II. Biophys Chem 130:102–113. doi:10.1016/j.bpc.2007.08.002

Lindahl E, Hess B, van der Spoel D (2001) GROMACS 3.0: a package for molecular simulation and trajectory analysis. J Mol Model 7:306–317

Luttmann E, Fels G (2006) All-atom molecular dynamics studies of the full-length beta-amyloid peptides. Chem Phys 323:138–147. doi:10.1016/j.chemphys.2005.08.071

Ma BY, Nussinov R (2002) Stabilities and conformations of Alzheimer's $\beta$-amyloid peptide oligomers (A$\beta$ 16–22, A$\beta$ 16–35, and A$\beta$ 10–35): sequence effects. PNAS USA 99:14126–14131. doi:10.1073/pnas.212206899

MacRaild CA, Hatters DM, Howlett GJ, Gooley PR (2001) NMR structure of human apolipoprotein C-II in the presence of sodium dodecyl sulfate. Biochemistry 40:5414–5421. doi:10.1021/bi002821m

MacRaild CA, Howlett GJ, Gooley PR (2004) The structure and interactions of human apolipoprotein C-II in dodecyl phosphocholine. Biochemistry 43:8084–8093. doi:10.1021/bi049817l

Mak PA, Laffitte BA, Desrumaux C, Joseph SB, Curtiss LK, Mangelsdorf DJ et al (2002) Regulated expression of the apolipoprotein E/C–I/C-IV/C-II gene cluster in murine and human macrophages—a critical role for nuclear liver X receptors alpha and beta. J Biol Chem 277:31900–31908. doi:10.1074/jbc.M202993200

Makin OS, Atkins E, Sikorski P, Johansson J, Serpell LC (2005) Molecular basis for amyloid fibril formation and stability. PNAS USA 102:315–320. doi:10.1073/pnas.0406847102

Maleknia SD, Reixach N, Buxbaum JN (2006) Oxidation inhibits amyloid fibril formation of transthyretin. FEBS J 273:5400–5406. doi:10.1111/j.1742-4658.2006.05532.x

Milner-White EJ, Watson JD, Qi GY, Hayward S (2006) Amyloid formation may involve alpha- to beta sheet interconversion via peptide plane flipping. Structure 14:1369–1376. doi:10.1016/j.str.2006.06.016

Naito A, Kamihira M, Inoue R, Saito H (2004) Structural diversity of amyloid fibril formed in human calcitonin as revealed by site-directed C-13 solid-state NMR spectroscopy. Magn Reson Chem 42:247–257. doi:10.1002/mrc.1323

Nelson R, Eisenberg D (2006) Recent atomic models of amyloid fibril structure. Curr Opin Struct Biol 16:260–265. doi:10.1016/j.sbi.2006.03.007

Nishino M, Sugita Y, Yoda T, Okamoto Y (2005) Structures of a peptide fragment of beta(2)-microglobulin studied by replica-exchange molecular dynamics simulations—towards the understanding of the mechanism of amyloid formation. FEBS Lett 579:5425–5429. doi:10.1016/j.febslet.2005.08.068

Palmblad M, Westlind-Danielsson A, Bergquist J (2002) Oxidation of methionine 35 attenuates formation of amyloid beta-peptide 1–40 oligomers. J Biol Chem 277:19506–19510. doi:10.1074/jbc.M112218200

Powers GA, Pham CLL, Pearce MC, Howlett GJ, Bottomley SP (2007) Serpin acceleration of amyloid fibril formation: a role for accessory proteins. J Mol Biol 366:666–676. doi:10.1016/j.jmb.2006.11.062

Reches M, Gazit E (2005) Self-assembly of peptide nanotubes and amyloid-like structures by charged-termini-capped diphenylalanine peptide analogues. Isr J Chem 45:363–371. doi:10.1560/5MC0-V3DX-KE0B-YF3J

Santini S, Derreumaux P (2004) Helix H1 of the prion protein is rather stable against environmental perturbations: molecular dynamics of mutation and deletion variants of PrP(90–231). Cell Mol Life Sci 61:951–960. doi:10.1007/s00018-003-3455-3

Sinha N, Tsai CJ, Nussinov R (2001) A proposed structural model for amyloid fibril elongation: domain swapping forms an interdigitating beta-structure polymer. Protein Eng 14:93–103. doi:10.1093/protein/14.2.93

Stewart CR, Haw A, Lopez R, McDonald TO, Callaghan JM, McConville MJ et al (2007) Serum amyloid P colocalizes with apolipoproteins in human atheroma: functional implications. J Lipid Res 48:2162–2171. doi:10.1194/jlr.M700098-JLR200

Tarus B, Straub JE, Thirumalai D (2006) Dynamics of Asp23-Lys28 salt-bridge formation in A beta(10–35) monomers. J Am Chem Soc 128:16159–16168. doi:10.1021/ja064872y

Thurlkill RL, Grimsley GR, Scholtz JM, Pace CN (2006) pK values of the ionizable groups of proteins. Protein Sci 15:1214–1218. doi:10.1110/ps.051840806

Tomaselli S, Esposito V, Vangone P, van Nuland NAJ, Bonvin AMJJ, Guerrini R et al (2006) The alpha-to-beta conformational transition of Alzheimer's A beta-(1–42) peptide in aqueous media is reversible: a step by step conformational analysis suggests the location of beta conformation seeding. ChemBioChem 7:257–267. doi:10.1002/cbic.200500223

Triguero L, Singh R, Prabhakar R (2008) Molecular dynamics study to investigate the effect of chemical substitutions of methionine 35 on the secondary structure of the amyloid beta (A beta(1–42)) monomer in aqueous solution. J Phys Chem B 112:2159–2167. doi:10.1021/jp0771872

Van der Spoel D, Lindahl E, Hess B, Groenhof G, Mark AE, Berendsen HJC (2005) GROMACS: fast, flexible, and free. J Comput Chem 26:1701–1718. doi:10.1002/jcc.20291

Wei GH, Shea JE (2006) Effects of solvent on the structure of the Alzheimer amyloid-beta(25–35) peptide. Biophys J 91:1638–1647. doi:10.1529/biophysj.105.079186

Wilson LM, Mok YF, Binger KJ, Griffin MDW, Mertens HDT, Lin F et al (2007) A structural core within apolipoprotein C-II amyloid fibrils identified using hydrogen exchange and proteolysis. J Mol Biol 366:1639–1651. doi:10.1016/j.jmb.2006.12.040

Wu C, Lei HX, Duan Y (2005) The role of Phe in the formation of well-ordered oligomers of amyloidogenic hexapeptide (NFGAIL) observed in molecular dynamics simulations with explicit solvent. Biophys J 88:2897–2906. doi:10.1529/biophysj.104.055574

Zdunek J, Martinez GV, Schleucher J, Lycksell PO, Yin Y, Nilsson S et al (2003) Global structure and dynamics of human apolipoprotein CII in complex with micelles: evidence for increased mobility of the helix involved in the activation of lipoprotein lipase. Biochemistry 42:1872–1889. doi:10.1021/bi0267184